

Enhanced s^\pm -wave superconductivity in electron-doped $\text{La}_3\text{Ni}_2\text{O}_7$

Xun Liu¹, Chao Deng², Wenfeng Wu³, Liang Si^{2,4,5,3} and Mi Jiang^{1,6,*}

¹*Institute for Quantum Science, School of Physical Science and Technology, Soochow University, Suzhou 215006, China*

²*School of Physics, Northwest University, Xi'an 710127, China*

³*Institute of Solid State Physics, TU Wien, 1040 Vienna, Austria*

⁴*Shaanxi Key Laboratory for Theoretical Physics Frontiers, Xi'an 710127, China*

⁵*Fundamental Discipline Research Center for Quantum Science and technology of Shaanxi Province, Xi'an 710127, China*

⁶*State Key Laboratory of Surface Physics and Department of Physics, Fudan University, Shanghai 200433, P. R. China*

In cuprates, electron doping yields a much lower superconducting T_c than hole doping. For recently discovered nickelate superconductors, the analogous doping strategies become more challenging. Consequently, while hole-doped Ruddlesden-Popper (RP) nickelates have been extensively studied, electron-doped RP nickelates remain rarely explored both experimentally and theoretically. Here we fill this gap by systematically investigating the two-orbital bilayer model for three representative systems: bulk $\text{La}_3\text{Ni}_2\text{O}_7$ at ambient pressure and 15 GPa, and a heterostructure $\text{La}_3\text{Ni}_2\text{O}_7:\text{La}_3\text{Al}_2\text{O}_7$ that provides a feasible experimental route to electron doping. Using first-principle calculations and large-scale dynamical cluster quantum Monte Carlo simulations, we find that electron doping generically enhances s^\pm -wave pairing superconductivity (SC) in all three cases, with the heterostructure showing the highest T_c in the underdoped regime. Furthermore, our results suggest an inter-orbital cooperative mechanism that the pairing on the $d_{x^2-y^2}$ orbital, induced by that on the d_{z^2} orbital, plays a vital role in the SC. This work provides the theoretical prediction of enhanced SC in electron-doped RP nickelates and calls for future experimental verification.

Introduction. The discovery of high-temperature superconductivity (SC) in cuprates [1–4] has long been a central theme in condensed matter physics. A hallmark of these layered oxides is the strong electron–hole asymmetry in their phase diagrams: under hole doping, a broad superconducting dome emerges with T_c reaching values above 100 K [5–7], whereas electron doping yields a much narrower superconducting region and a significantly suppressed T_c [8]. This asymmetry mostly originates from the different electronic structures of hole- and electron-doped Fermi surfaces. Technically, in hole-doped cuprates, substitution of trivalent A -site cations (La^{3+} , Nd^{3+} or Pr^{3+}) by divalent cations (e.g., Ca^{2+} , Sr^{2+} or Ba^{2+}) introduces holes into the CuO_2 planes in cuprates such as La_2CuO_4 [9, 10]. Electron doping, on the other hand, is typically realized by replacing trivalent rare-earth ions (La^{3+} , Nd^{3+} or Pr^{3+}) with tetravalent Ce^{4+} (e.g., in $\text{Nd}_{2-x}\text{Ce}_x\text{CuO}_4$) [8, 11] or by substituting divalent A -site cations with trivalent ions (e.g., Nd^{3+} or La^{3+} in place of Sr^{2+} or Ca^{2+}) [12, 13].

In sharp contrast to cuprates, the recently discovered nickelate superconductors, including the infinite-layer family $R\text{NiO}_2$ ($R=\text{La}$, Nd or Pr) [15–17] and the Ruddlesden-Popper (RP) phases $\text{La}_3\text{Ni}_2\text{O}_7$ [18–22] and $\text{La}_4\text{Ni}_3\text{O}_{10}$ [23–25], present a very different doping landscape. The nickel’s trivalent (Ni^{3+}) or divalent (Ni^{2+}) oxidation states make it difficult to directly transplant the electron-doping schemes developed for cuprates. Few elements (such as Ce) can reliably adopt a stable +4 oxidation state under the relevant synthesis

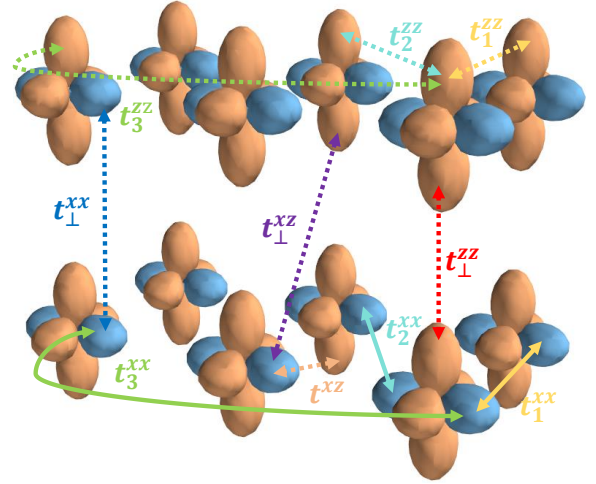


FIG. 1. Schematic illustration of the bilayer two-orbital model on a square lattice. The model incorporates three types of hoppings: (1) intralayer intra-orbital hoppings: nearest-neighbor ($t_1^{xx/zz}$), next-nearest-neighbor ($t_2^{xx/zz}$), and next-next-nearest-neighbor ($t_3^{xx/zz}$); (2) intralayer inter-orbital hopping (t^{xz}); and (3) interlayer hoppings: intra-orbital ($t_\perp^{xx/zz}$) and inter-orbital (t_\perp^{xz}). The values of these parameters for 0 GPa, 15 GPa and $\text{LaNi}(\text{Al})\text{O}$ are listed in Table. S1 in Supplementary [14].

conditions, however, the electrons from $\text{Ce-}4f$ orbital lie energetically much deeper (by several eV) than the $\text{Ni-}3d$ electrons, hence Ce substitution does not effectively transfer/dope electrons into the e_g orbital in Ni^{2+} or Ni^+ . Consequently, the recently reported experimental

* jiangmi@suda.edu.cn

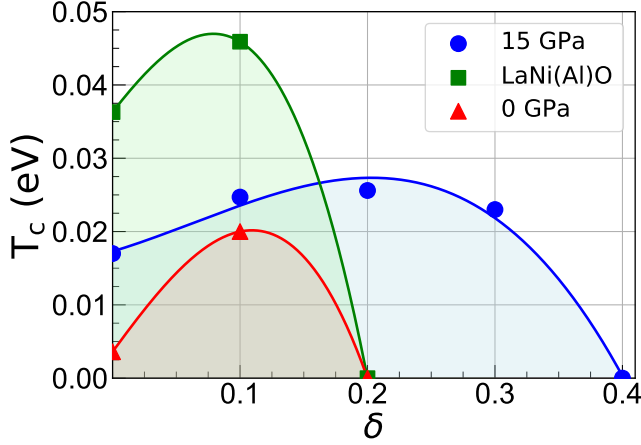


FIG. 2. Extrapolated T_c as a function of electron doping level δ for three different cases with the $N_c = 4 \times 2$ cluster.

studies on RP phase nickelates have so far been focused on samples with hole doping, typically by partially substituting La^{3+} with Sr^{3+} to simultaneously stabilize the lattice structure and introduce holes into the NiO_2 planes [26–28]. Electron-doped RP nickelates remain almost completely unexplored experimentally and rarely discussed theoretically.

Given that electron doping in cuprates already yields unconventional SC (albeit with lower T_c) and that the nickelate’s electronic structure shares important similarities (and also differences such as the interstitial- s orbital [29–31] and pocket bands) with that of cuprates (e.g., quasi-two-dimensional $d_{x^2-y^2}$ -derived Fermi surfaces), it becomes imperative and essential to raise the question: can electron doping also induce or even enhance SC in RP nickelates? To answer this question, we need not only a viable experimental route to electron doping, but also a reliable (many-body level) theoretical framework to compute the superconducting properties beyond conventional mean-field approximations such as density-functional theory (DFT).

In this work, we perform large-scale many-body calculation toward filling this gap. We construct a (minimal) two-orbital bilayer tight-binding model that captures the low-energy physics of three distinct systems: (i) bulk $\text{La}_3\text{Ni}_2\text{O}_7$ at ambient pressure (0 GPa), (ii) the same compound under 15 GPa where SC has been observed experimentally [18], and (iii) a heterostructure $\text{La}_3\text{Ni}_2\text{O}_7:\text{La}_3\text{Al}_2\text{O}_7$ (LaNi(Al)O) [32]. The latter is designed to achieve electron doping via charge transfer from the insulating $\text{La}_3\text{Al}_2\text{O}_7$ spacer layers. Using first-principles density functional theory (DFT) [33–40] to obtain accurate hopping parameters and employing large-scale dynamical cluster quantum Monte Carlo (QMC) simulations to treat strong correlations, we systematically study the pairing tendencies in these electron-doped systems. We find that electron doping

universally enhances s^\pm -wave pairing SC in all three cases, with the heterostructured LaNi(Al)O exhibiting the highest T_c in the underdoped regime. Moreover, our results reveal an inter-orbital cooperative mechanism: the s^\pm -wave pairing on the $3d_{x^2-y^2}$ orbital appears to be induced by that on the Ni- $3d_{z^2}$ orbital. This work not only provides the theoretical prediction of enhanced SC in electron-doped RP nickelates but also proposes a concrete and experimentally feasible heterostructure design to realize it, stimulating future experimental efforts to explore the rich and largely uncharted electron-doped side of nickelate superconductors.

Model. We consider the bilayer two-orbital model for the bulk $\text{La}_3\text{Ni}_2\text{O}_7$ on a two-dimensional square lattice as shown in Fig. 1 with the Hamiltonian

$$\begin{aligned}
 H &= H_0 + H_U \\
 H_0 &= \sum_{ij\sigma m l\nu} t_\nu^{xx/zz} c_{iml\sigma}^\dagger c_{jml\sigma} + t^{xz} \sum_{\langle ij \rangle \sigma m l l'} c_{iml\sigma}^\dagger c_{jml'\sigma} \\
 &\quad + t_\perp^{xz} \sum_{\langle ij \rangle l l' \sigma} c_{i1l\sigma}^\dagger c_{j2l'\sigma} + t_\perp^{xx/zz} \sum_{i l \sigma} c_{i1l\sigma}^\dagger c_{i2l\sigma} \\
 &\quad + (\epsilon^{x/z} - \mu) \sum_{iml\sigma} n_{iml\sigma} + \text{H.c.} \\
 H_U &= U \sum_{iml} n_{iml\uparrow} n_{iml\downarrow} + U' \sum_{iml'\sigma\sigma'} n_{iml\sigma} n_{iml'\sigma'} \\
 &\quad + (U' - J) \sum_{iml l' \sigma} n_{iml\sigma} n_{iml' \sigma}
 \end{aligned}$$

where $c_{i\sigma}^\dagger$ ($c_{i\sigma}$) creates (annihilates) an electron at site i in layer $m = 1, 2$ with spin $\sigma = \uparrow, \downarrow$ and orbital $l = d_{x^2-y^2}(x)$ or $d_{z^2}(z)$. The hoppings $t_\nu^{xx/zz}$ include nearest-, next-nearest-, and next-next-nearest-neighbor terms $t_1^{xx/zz}$, $t_2^{xx/zz}$, $t_3^{xx/zz}$ for the two orbitals. $t_\perp^{xx/zz}$ are interlayer intra-orbital hoppings, and t^{xz} , t_\perp^{xz} are intralayer and interlayer inter-orbital hoppings. The tight-binding parameters (from DFT) are listed in Table. S1 and the non-interacting band structure shown in Fig. S1 in Supplementary [14]. The on-site Coulomb interaction is $U = 4.0$ eV, inter-orbital $U' = U - 2J = 2.4$ eV with Hund’s coupling $J = U/5 = 0.8$ eV. The chemical potential μ tunes the average total density n per bilayer e_g orbitals, with electron-doping level $\delta = n - 3.0$, and the density distribution is presented in Fig. S2 in Supplementary [14]. The model is solved using dynamical cluster approximation (DCA) with CT-QMC cluster solver [41–44]. The superconducting properties are obtained by solving the Bethe-Salpeter equation (BSE) in the particle-particle channel [45, 46]. Further details on the methodology are presented in Supplementary [14].

Our main results for the superconducting properties are presented in two parts, based on different cluster size used in the calculations: (A) $N_c = 4 \times 2$ -site cluster via the BSE; (B) $N_c = 1 \times 2$ -site cluster via the pair-field susceptibility. Importantly, the s^\pm -wave pairing SC is generally enhanced by electron doping, irrespective of the cluster size.

SC with $N_c = 4 \times 2$. The main result is summarized in the phase diagram shown in Fig. 2. For all three cases, the s^\pm -wave pairing SC exhibits a dome-like dependence of T_c on electron doping. Notably, even at 0 GPa, where almost no SC exists without doping, a dome-like T_c emerges upon electron doping, peaking around optimal $\delta \approx 0.1$ and ultimately disappearing near $\delta \approx 0.2$. For 15 GPa, the T_c dome is wider, with an optimal doping of $\delta \approx 0.2$, which agrees with previous slave-boson mean-field results [47, 48], where electron doping under pressure also enhances SC. In the LaNi(Al)O case, SC exists without doping and is enhanced by electron doping, with a rapid T_c rise and decay than that of 15 GPa. Therefore, via electron doping, LaNi(Al)O at ambient pressure can achieve a higher T_c than pressurized $\text{La}_3\text{Ni}_2\text{O}_7$ (e.g., at $\delta = 0.1$ of blue line in Fig. 2). Although the T_c with $N_c = 4$ per layer might be overestimated [49], particularly the low but finite T_c at ambient pressure (red line) without doping contradicts with the experimental observation, the qualitative doping evolution should be trustworthy.

The eigenvectors presented in Fig. 3 correspond to the lowest accessible temperatures for two representative cases: (left) LaNi(Al)O with $\delta = 0.1$ and (right) 15 GPa with $\delta = 0.3$. In both cases, the dominant pairing arises from the d_{z^2} orbital. The fact that the interlayer component $z^1 z^2$ exceeds the intralayer components $z^1 z^1$ is a clear signature of s^\pm -wave pairing symmetry. Furthermore, in the 15 GPa case, the pairing components associated with the $d_{x^2-y^2}$ orbital also exhibit a weaker s^\pm -wave pairing. This is likely induced by the d_{z^2} orbital through inter-orbital hybridization [50] and/or Hund's coupling [48, 51, 52]. As discussed next, the features are more pronounced in $N_c = 1 \times 2$ results at lower temperatures.

The T_c shown in Fig. 2 are obtained by extrapolating the BSE eigenvalues using either a logarithmic function ($\sim A \log(T/T_c)$) or a linear function ($\sim A(T - T_c)$) [53, 54]. More details are given in the Supplementary [14]. As shown in Fig. 4, although the achievable temperature range is limited by the QMC sign problem, the extrapolated T_c using the appropriate fitting functions can still provide at least qualitatively reasonable doping dependent tendency. Specifically, for the 15 GPa and 0 GPa cases, T_c is extrapolated linearly at $\delta = 0.4$ and $\delta = 0.2$, respectively, while a logarithmic function is used for the remaining doping levels. For the LaNi(Al)O case, T_c is extrapolated using a linear function.

SC with $N_c = 1 \times 2$. To explore the superconducting properties at lower temperature scale, we reduce the cluster size to $N_c = 1 \times 2$ to examine the orbital-resolved pair-field susceptibility [55–58] for 15 GPa and LaNi(Al)O cases.

As shown in Fig. 5(a), with the temperature decreasing to $T = 0.01$ eV, the inverse s^\pm -wave pair-field susceptibility $P^{-1}(T)$ approaches to zero or becomes negative. For the former, we can extrapolate T_c by linearly fitting $P^{-1}(T)$ at the two lowest temperatures;

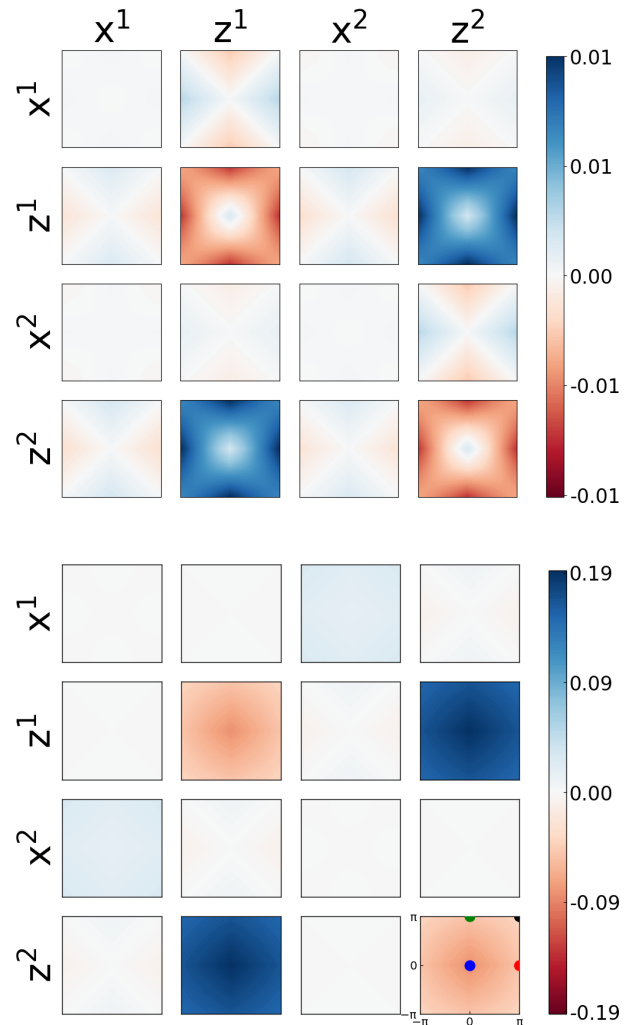


FIG. 3. Characteristic BSE eigenvectors revealing stronger interlayer pairing for two distinct cases at their lowest accessible temperatures: (left) LaNi(Al)O with electron doping level $\delta = 0.1$ at $T = 0.06$ eV; (right) 15 GPa with $\delta = 0.3$ at $T = 0.09$ eV. The label l^m denotes orbital l in layer m and the Γ , X and M points are denoted by purple, red and black circles respectively.

while for the latter, the negative $P^{-1}(T)$ indicates that $P(T)$ has diverged, which is used to estimate T_c . The corresponding T_c is presented in the inset of Fig. 5(a). For the 15 GPa case, a dome-like behavior is observed with a wider electron-doping regime compared to the T_c shown in Fig. 2. For the LaNi(Al)O case, although T_c is also higher than that of the 15 GPa case at $\delta = 0.0$ and 0.1, the dome-like behavior disappears, and instead a half-dome behavior is observed over a wide doping regime. The discrepancy of T_c curves between $N_c = 4 \times 2$ and $N_c = 1 \times 2$ might originate from the uncertainty of T_c estimation from different temperature ranges, especially for the elevated temperature simulations for $N_c = 4 \times 2$. Another possibility is the spatial correlation included in $N_c = 4 \times 2$ cluster has apparent impact on the

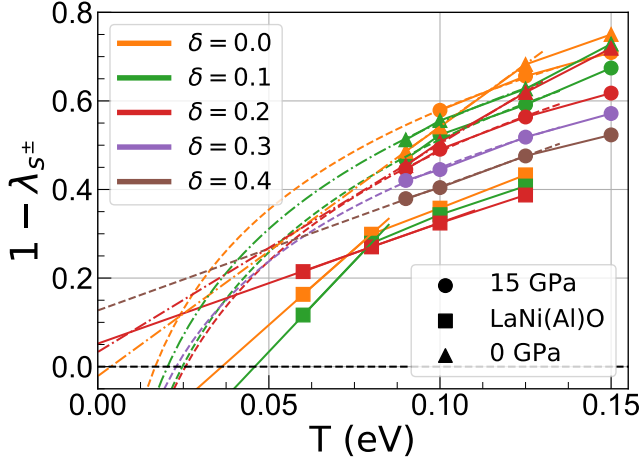


FIG. 4. Temperature dependence of the eigenvalue $1 - \lambda_{s^{\pm}}$ for extrapolating T_c under three distinct conditions: 15 GPa (circles) with doping levels $\delta = 0.0, 0.1, 0.2, 0.3, 0.4$; and 0 GPa (squares) and LaNi(Al)O (triangles) both with $\delta = 0.0, 0.1, 0.2$.

T_c scale and its corresponding doping evolution. In essence, our simulations using two different cluster sizes are complement to each other.

As discussed in detail in the Supplementary [14], the pair-field susceptibility can be decomposed into the non-interacting and interacting parts for both intra- and inter-orbital components. Generally, the temperature evolution of the interacting part $P_{\Gamma}(T)$ is crucial for understanding the correlation induced SC instability [58]. Fig. 5(b) presents the difference between $P_{\Gamma}^x(T)$ and $P_{\Gamma}^z(T)$ for $\delta = 0.0, 0.2$, and 0.4 , respectively. Clearly, as the temperature lowers, $P_{\Gamma}^x(T)$ increases rapidly and eventually surpasses $P_{\Gamma}^z(T)$; while $P_{\Gamma}^z(T)$ remains almost unchanged for both the 15 GPa and LaNi(Al)O cases, which strongly indicates that the more itinerant $d_{x^2-y^2}$ orbital plays a vital role in the interlayer pairing SC in $\text{La}_3\text{Ni}_2\text{O}_7$.

Moreover, although there is no momentum resolution for $N_c = 1 \times 2$ cluster, we can explore the representative eigenvector weight η , which is defined as the absolute value of a given eigenvector component ($\phi_{\parallel}^{xx}, \phi_{\perp}^{xx}, \phi_{\parallel}^{zz}, \phi_{\perp}^{zz}$) at lowest Matsubara frequency normalized by the summation of all four. As a representative example, Fig. 5(c) displays the temperature evolution of these weights for the 15 GPa case at $\delta = 0.2$. More results are shown in the Supplementary [14]. Fig. 5(c) illustrates that, at relatively high temperature range above $T > 0.08$ eV, the intralayer ϕ_{\parallel}^{zz} of the d_{z^2} orbital decreases while its interlayer counterpart ϕ_{\perp}^{zz} increases, signaling a crossover from intralayer to interlayer pairing. However, with further lowering T below $T = 0.08$ eV, the interlayer ϕ_{\perp}^{zz} starts to weaken and simultaneously the $d_{x^2-y^2}$ orbital plays a more and more important role before finally exceeding the contribution from d_{z^2} orbital. Apparently, the interlayer ϕ_{\perp}^{xx} dominates over the intralayer ϕ_{\parallel}^{xx} .

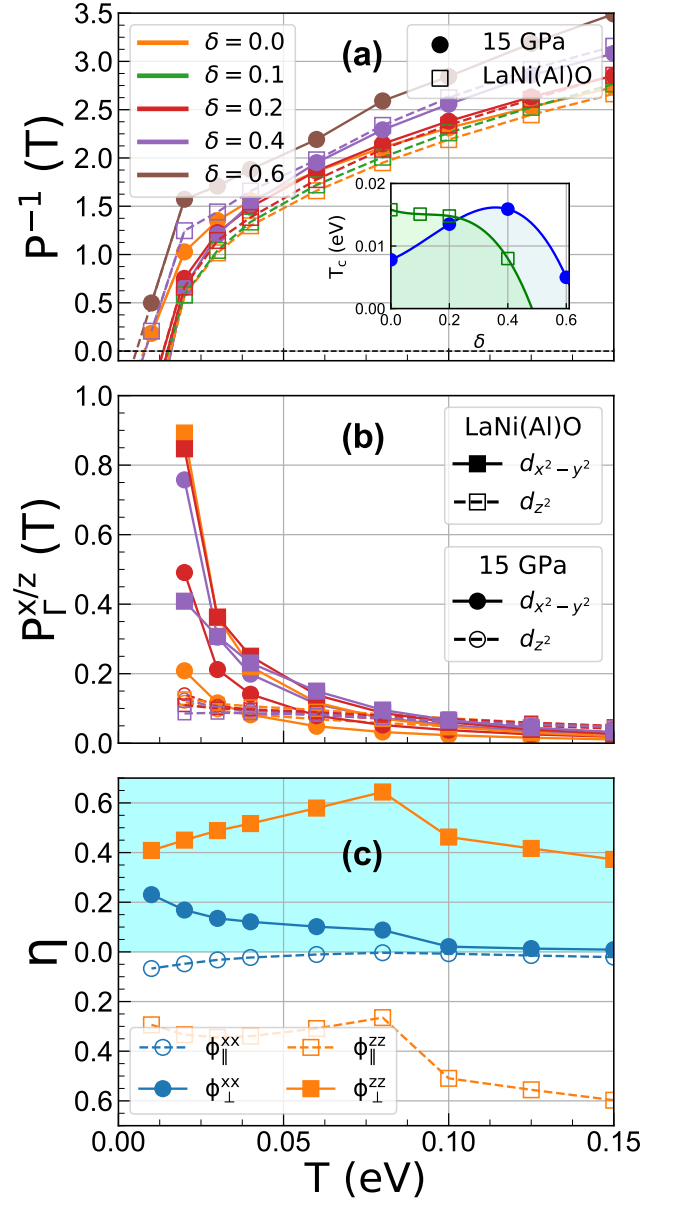


FIG. 5. (a) Temperature dependence of the inverse of s^{\pm} -wave pair-field susceptibility $P^{-1}(T)$ for the 15 GPa and LaNi(Al)O cases under different electron doping levels δ . The inset shows the corresponding extrapolated T_c obtained from $P^{-1}(T_c) = 0$; (b) Orbital-resolved components (P_{Γ}^x and P_{Γ}^z) of the interacting part of s^{\pm} -wave pair-field susceptibility at $\delta = 0.0, 0.2$, and 0.4 for both cases; (c) Characteristic temperature evolution of the weights η (defined in the main text) for the orbital-resolved intralayer ($\phi_{\parallel}^{xx/z^z}$) and interlayer (ϕ_{\perp}^{xx/z^z}) eigenvector for the 15 GPa case at $\delta = 0.2$.

Both Fig. 5(b-c) suggest that the pairing in the $d_{x^2-y^2}$ orbital becomes more significant than d_{z^2} orbital at low temperature but the pairing may originate from the d_{z^2} orbital although the exact mechanism is unclear yet [48, 50–52, 59] and deserves more extensive investigation.

Summary and Outlook. How to achieve electron doping in lanthanum-nickelate superconductors, and the resulting effects on their physical properties, remain key open questions from both experimental and theoretical perspectives. In the current research, we systematically investigated the superconducting properties of the two-orbital bilayer model for $\text{La}_3\text{Ni}_2\text{O}_7$ under electron doping, considering $\text{La}_3\text{Ni}_2\text{O}_7$ at three distinct conditions: bulk $\text{La}_3\text{Ni}_2\text{O}_7$ at ambient pressure, bulk $\text{La}_3\text{Ni}_2\text{O}_7$ at 15 GPa, and a disorder-free heterostructure $\text{La}_3\text{Ni}_2\text{O}_7:\text{La}_3\text{Al}_2\text{O}_7$ [denoted $\text{LaNi}(\text{Al})\text{O}$] that offers a feasible route to electron doping.

Using large-scale dynamical cluster approximation (DCA) quantum Monte Carlo simulations with a continuous-time quantum Monte Carlo cluster solver, and employing cluster sizes $N_c = 4 \times 2$ and 1×2 , we provide robust numerical evidence that electron doping universally enhances s^\pm -wave pairing superconductivity, and T_c exhibits a dome-like dependence on doping concentration—reminiscent of electron-doped two-dimensional cuprate superconductors [60]. Notably, the $\text{LaNi}(\text{Al})\text{O}$ heterostructure, a feasible experimental platform for electron doping, shows the highest T_c in the underdoped regime. Consistent results are also obtained with the smaller cluster size $N_c = 1 \times 2$ at lower temperatures, confirming the stability of our conclusions.

Next, the temperature evolution of the orbital-resolved pair-field susceptibility and its eigenvector indicates that the $d_{x^2-y^2}$ orbital plays a more dominant role in s^\pm -wave pairing. Nevertheless, the s^\pm -wave pairing on the $d_{x^2-y^2}$ orbital at low temperatures may be induced by that on the d_{z^2} orbital, implying a two-orbital cooperative mechanism behind the superconducting instability in $\text{La}_3\text{Ni}_2\text{O}_7$ —a mechanism that cannot be captured by the single-band ($d_{x^2-y^2}$) approximation successfully applied to infinite-layer nickelates [61–63]. In this two-band model, the inter-orbital coupling between $d_{x^2-y^2}$ and d_{z^2} may arise from three possible origins: inter-orbital Hund’s coupling [48, 51, 52], inter-orbital hybridization [50], or a combination of both. The

Hund’s coupling mechanism is more suitable for integer electron occupancy (i.e., the undoped case), whereas inter-orbital hybridization becomes relevant for doped systems, consistent with earlier studies on hole-doped $\text{La}_3\text{Ni}_2\text{O}_7$ [59].

Although our many-body calculations show that electron doping can enhance the superconducting transition temperature, experimental realization remains challenging. The Ce-doping approach, successful in electron-doped cuprates [60], is ineffective in nickelates because the Ce-4*f* electrons lie at much lower energy, making electron transfer into Ni-*e_g* orbital. The proposed heterostructure route requires the synthesis of stable $\text{La}_3\text{Ni}_2\text{O}_7$ layers and the prevention of intermixing between Ni and Al, which also presents significant experimental difficulties. Aside from the heterostructuring way, another possible route to electron doping is hydrogen (H) intercalation. Recent theoretical work [64] has shown that H-intercalation into La_2NiO_4 successfully achieves electron doping, resulting in a $3d^9$ electronic configuration, a single-band $d_{x^2-y^2}$ Fermi surface, an antiferromagnetic Mott insulating ground state—analogueous to the parent cuprate La_2CuO_4 —and superconductivity upon hole doping. Hence, (proton) ionic gating (e.g., H^+) may provide an alternative way to realize electron doping in bulk and thin film $\text{La}_3\text{Ni}_2\text{O}_7$, awaiting future experimental verification.

Acknowledgment. X. Liu and M. Jiang acknowledge the support of the National Natural Science Foundation of China (Grant No.12174278) and State Key Laboratory of Surface Physics and Department of Physics in Fudan University (Grant No.KF2025-12). C. Deng, W. Wu, and L. Si acknowledge support from the National Natural Science Foundation of China (Grant No. 12422407) and the Key Research and Development Program of Shaanxi (2024QY2-GJHX-42). M. Jiang also acknowledges the support of the China Scholarship Council (CSC) and the hospitality of Karsten Held at TU Wien. Calculations have been mainly done in Soochow University and the National Supercomputing Center (Xi’an) in Northwest University.

-
- [1] J. G. Bednorz and K. A. Müller, Possible high T_c superconductivity in the Ba-La-Cu-O system, *Zeitschrift für Physik B Condensed Matter* **64**, 189 (1986).
 - [2] C. C. Tsuei and J. R. Kirtley, Pairing symmetry in cuprate superconductors, *Rev. Mod. Phys.* **72**, 969 (2000).
 - [3] A. Damascelli, Z. Hussain, and Z.-X. Shen, Angle-resolved photoemission studies of the cuprate superconductors, *Rev. Mod. Phys.* **75**, 473 (2003).
 - [4] L. Deng, T. Habamahoro, A. Safezoddeh, B. Karki, S. Kazibwe, D. J. Schulze, Z. Wu, M. Julian, R. P. Prasankumar, H. Zhou, J. S. Smith, P. R. Hosur, and C.-W. Chu, Ambient-pressure 151 K superconductivity in $\text{HgBa}_2\text{Ca}_2\text{Cu}_3\text{O}_{8+\delta}$ via pressure quench, *Proceedings of the National Academy of Sciences* **123** (2026).
 - [5] J. M. G. A Conde, G. C Falcony, and S. V, Tl-based superconductors for high-current, high-field applications, *Superconductor Science and Technology* **9**, 427 (1996).
 - [6] A. Schilling, M. Cantoni, J. D. Guo, and H. R. Ott, Superconductivity above 130 K in the Hg–Ba–Ca–Cu–O system, *Nature* **363**, 1476 (1993).
 - [7] T. Kawashima, Y. Matsui, and M. E. Takayama, New oxycarbonate superconductors $(\text{Cu}_{0.5}\text{Co}_{0.5})\text{Ba}_2\text{Ca}_{n-1}\text{Cu}_n\text{O}_{2n+3}$ ($n = 3, 4$) prepared at high pressure, *Physica C: Superconductivity* **224**, 69 (1994).
 - [8] N. P. Armitage, P. Fournier, and R. L. Greene, Progress and perspectives on electron-doped cuprates, *Rev. Mod. Phys.* **82**, 2421 (2010).
 - [9] P. W. Anderson, The resonating valence bond state in

- la₂cuo₄ and superconductivity, *science* **235**, 1196 (1987).
- [10] J. Attfield, A. Kharlanov, and J. McAllister, Cation effects in doped la₂cuo₄ superconductors, *Nature* **394**, 157 (1998).
- [11] H. Takagi, S. Uchida, and Y. Tokura, Superconductivity produced by electron doping in CuO₂-layered compounds, *Phys. Rev. Lett.* **62**, 1197 (1989).
- [12] M. Smith, A. Manthiram, J. Zhou, J. Goodenough, and J. Markert, Electron-doped superconductivity at 40 k in the infinite-layer compound sr_{1-y}ndycu_{0.2}, *nature* **351**, 549 (1991).
- [13] A. Ikeda, Y. Krockenberger, and H. Yamamoto, Molecular beam epitaxy of electron-doped infinite-layer ca_{1-x}R_xcuo₂ thin films, *Phys. Rev. Mater.* **3**, 064803 (2019).
- [14] See Supplementary Material at <http://link...> for: (1) further details on the methodology in Section. S.I, (2) non-interacting band structures and density distribution in Section. S.II, and (3) a more detailed analysis of the temperature evolution of the eigenvectors for $N_c = 1 \times 2$ in Section. S.III.
- [15] D. Li, K. Lee, B. Y. Wang, M. Osada, S. Crossley, H. R. Lee, Y. Cui, Y. Hikita, and H. Y. Hwang, Superconductivity in an infinite-layer nickelate, *Nature* **572**, 624 (2019).
- [16] S. Zeng, C. Li, L. E. Chow, Y. Cao, Z. Zhang, C. S. Tang, X. Yin, Z. S. Lim, J. Hu, P. Yang, and A. Ariando, Superconductivity in infinite-layer nickelate la_{1-x}ca_xnio₂ thin films, *Science Advances* **8**, eabl9927 (2022).
- [17] S. Wenjie, J. Zhicheng, X. Chengliang, H. Bo, Y. Shengjun, W. Maosen, L. Yueying, L. Hongquan, D. Jianyang, L. Jiayu, L. Zhengtai, L. Jishan, C. Hanghui, S. Dawei, and N. Yuefeng, Electronic structure of superconducting infinite-layer lanthanum nickelates, *Science Advances* **11**, eadr5116 (2025).
- [18] H. Sun, M. Huo, X. Hu, J. Li, Z. Liu, Y. Han, L. Tang, Z. Mao, P. Yang, B. Wang, J. Cheng, D.-X. Yao, G.-M. Zhang, and M. Wang, Signatures of superconductivity near 80 K in a nickelate under high pressure, *Nature* **621**, 493 (2023).
- [19] Y. Zhang, D. Su, Y. Huang, Z. Shan, H. Sun, M. Huo, K. Ye, J. Zhang, Z. Yang, Y. Xu, Y. Su, R. Li, M. Smidman, M. Wang, L. Jiao, and H. Yuan, High-temperature superconductivity with zero resistance and strange-metal behaviour in La₃Ni₂O_{7- δ} , *Nature Physics* **20**, 1269 (2024).
- [20] G. Wang, N. N. Wang, X. L. Shen, J. Hou, L. Ma, L. F. Shi, Z. A. Ren, Y. D. Gu, H. M. Ma, P. T. Yang, Z. Y. Liu, H. Z. Guo, J. P. Sun, G. M. Zhang, S. Calder, J.-Q. Yan, B. S. Wang, Y. Uwatoko, and J.-G. Cheng, Pressure-Induced Superconductivity In Polycrystalline La₃Ni₂O_{7- δ} , *Phys. Rev. X* **14**, 011040 (2024).
- [21] M. Zhang, C. Pei, Q. Wang, Y. Zhao, C. Li, W. Cao, S. Zhu, J. Wu, and Y. Qi, Effects of pressure and doping on Ruddlesden-Popper phases La_{n+1}Ni_nO_{3n+1}, *Journal of Materials Science and Technology* **185**, 147 (2024).
- [22] N. Wang, G. Wang, X. Shen, J. Hou, J. Luo, X. Ma, H. Yang, L. Shi, J. Dou, J. Feng, J. Yang, Y. Shi, Z. Ren, H. Ma, P. Yang, Z. Liu, Y. Liu, H. Zhang, X. Dong, Y. Wang, K. Jiang, J. Hu, S. Nagasaki, K. Kitagawa, S. Calder, J. Yan, J. Sun, B. Wang, R. Zhou, Y. Uwatoko, and J. Cheng, Bulk high-temperature superconductivity in pressurized tetragonal La₂PrNi₂O₇, *Nature* **634**, 579 (2024).
- [23] Y. Zhu, D. Peng, E. Zhang, B. Pan, X. Chen, L. Chen, H. Ren, F. Liu, Y. Hao, N. Li, Z. Xing, F. Lan, J. Han, J. Wang, D. Jia, H. Wo, Y. Gu, Y. Gu, L. Ji, W. Wang, H. Gou, Y. Shen, T. Ying, X. Chen, W. Yang, H. Cao, C. Zheng, Q. Zeng, J.-g. Guo, and J. Zhao, Superconductivity in pressurized trilayer La₄Ni₃O_{10- δ} single crystals, *Nature* **631**, 521 (2024).
- [24] M. Zhang, C. Pei, D. Peng, X. Du, W. Hu, Y. Cao, Q. Wang, J. Wu, Y. Li, H. Liu, C. Wen, J. Song, Y. Zhao, C. Li, W. Cao, S. Zhu, Q. Zhang, N. Yu, P. Cheng, L. Zhang, Z. Li, J. Zhao, Y. Chen, C. Jin, H. Guo, C. Wu, F. Yang, Q. Zeng, S. Yan, L. Yang, and Y. Qi, Superconductivity in Trilayer Nickelate La₄Ni₃O₁₀ under Pressure, *Phys. Rev. X* **15**, 021005 (2025).
- [25] Q. Li, Y.-J. Zhang, Z.-N. Xiang, Y. Zhang, X. Zhu, and H.-H. Wen, Signature of Superconductivity in Pressurized La₄Ni₃O₁₀, *Chinese Physics Letters* **41**, 017401 (2024).
- [26] B. Hao, M. Wang, W. Sun, Y. Yang, Z. Mao, S. Yan, H. Sun, H. Zhang, L. Han, Z. Gu, J. Zhou, D. Ji, and Y. Nie, Superconductivity in Sr-doped La₃Ni₂O₇ thin films, *Nature Materials* **24**, 1756 (2025).
- [27] Y. Wang, K. Jiang, J. Ying, T. Wu, J. Cheng, J. Hu, and X. Chen, Recent progress in nickelate superconductors, *National Science Review* **12**, nwaf373 (2025).
- [28] Y. Liu, B. Y. Wang, J. Li, Y. Tarn, L. Bhatt, M. Colletta, Y.-M. Wu, C.-T. Kuo, J.-S. Lee, B. H. Goodge, D. A. Muller, Z.-X. Shen, S. Raghu, H. Y. Hwang, and Y. Yu, A superconducting half-dome in bilayer nickelates, [arXiv:2603.12196](https://arxiv.org/abs/2603.12196).
- [29] Y. Nomura, M. Hirayama, T. Tadano, Y. Yoshimoto, K. Nakamura, and R. Arita, Formation of a two-dimensional single-component correlated electron system and band engineering in the nickelate superconductor ndnio₂, *Phys. Rev. B* **100**, 205138 (2019).
- [30] Y. Gu, S. Zhu, X. Wang, J. Hu, and H. Chen, A substantial hybridization between correlated ni-d orbital and itinerant electrons in infinite-layer nickelates, *Communications Physics* **3**, 84 (2020).
- [31] J.-Y. You, Interstitial *s* states and chemical pressure as key drivers of enhanced electron-phonon coupling in infinite-layer nickelates, *Phys. Rev. B* **113**, 064510 (2026).
- [32] C. Deng, M. Kitatani, G. Jiang, S. Guo, N. Witt, A. Zhang, W. Wu, M. Jiang, K. Held, and L. Si, Heterostructuring as gateway to electron doping of nickelate superconductors (2026), under preparation.
- [33] P. Hohenberg and W. Kohn, Inhomogeneous Electron Gas, *Phys. Rev.* **136**, B864 (1964).
- [34] W. Kohn and L. J. Sham, Self-Consistent Equations Including Exchange and Correlation Effects, *Phys. Rev.* **140**, A1133 (1965).
- [35] P. E. Blöchl, Projector augmented-wave method, *Phys. Rev. B* **50**, 17953 (1994).
- [36] G. Kresse and J. Furthmüller, Efficiency of ab-initio total energy calculations for metals and semiconductors using a plane-wave basis set, *Computational Materials Science* **6**, 15 (1996).
- [37] G. Kresse and J. Furthmüller, Efficient iterative schemes for ab initio total-energy calculations using a plane-wave basis set, *Phys. Rev. B* **54**, 11169 (1996).
- [38] P. Blaha, K. Schwarz, G. Madsen, D. Kvasnicka, and J. Luitz, *Wien2k: An augmented plane wave plus local*

- orbitals program for calculating crystal properties (2001).
- [39] K. Schwarz, P. Blaha, and G. Madsen, Electronic structure calculations of solids using the WIEN2k package for material sciences, *Computer Physics Communications* **147**, 71 (2002), proceedings of the Europhysics Conference on Computational Physics Computational Modeling and Simulation of Complex Systems.
- [40] J. P. Perdew, K. Burke, and M. Ernzerhof, Generalized Gradient Approximation Made Simple, *Phys. Rev. Lett.* **77**, 3865 (1996).
- [41] M. H. Hettler, A. N. Tahvildar-Zadeh, M. Jarrell, T. Pruschke, and H. R. Krishnamurthy, Nonlocal dynamical correlations of strongly interacting electron systems, *Phys. Rev. B* **58**, R7475 (1998).
- [42] T. Maier, M. Jarrell, T. Pruschke, and M. H. Hettler, Quantum cluster theories, *Rev. Mod. Phys.* **77**, 1027 (2005).
- [43] U. R. Hähner, G. Alvarez, T. A. Maier, R. Solcà, P. Staar, M. S. Summers, and T. C. Schulthess, DCA++: A software framework to solve correlated electron problems with modern quantum cluster methods, *Computer Physics Communications* **246**, 106709 (2020).
- [44] E. Gull, P. Werner, O. Parcollet, and M. Troyer, Continuous-time auxiliary-field monte carlo for quantum impurity models, *Europhysics Letters* **82**, 57003 (2008).
- [45] T. A. Maier, M. S. Jarrell, and D. J. Scalapino, Structure of the pairing interaction in the two-dimensional Hubbard model, *Phys. Rev. Lett.* **96**, 047005 (2006).
- [46] D. J. Scalapino, *Handbook of High-Temperature Superconductivity: Theory and Experiment* (Springer, New York, NY, 2007) pp. 495–526.
- [47] J.-H. Ji, C. Lu, Z.-Y. Shao, Z. Pan, F. Yang, and C. Wu, Strong-coupling study of the pairing mechanism in pressurized $\text{La}_3\text{Ni}_2\text{O}_7$, *Phys. Rev. B* **112**, 214515 (2025).
- [48] Z. Chen, J.-H. Ji, Y.-B. Liu, M. Zhang, and F. Yang, A Unified Understanding of the Experimental Controlling of the T_c of $\text{La}_3\text{Ni}_2\text{O}_7$, [arXiv:2603.14519](https://arxiv.org/abs/2603.14519).
- [49] T. A. Maier, M. Jarrell, T. C. Schulthess, P. R. C. Kent, and J. B. White, Systematic Study of d -Wave Superconductivity in the 2D Repulsive Hubbard Model, *Phys. Rev. Lett.* **95**, 237001 (2005).
- [50] Y.-F. Yang, G.-M. Zhang, and F.-C. Zhang, Interlayer valence bonds and two-component theory for high- T_c superconductivity of $\text{La}_3\text{Ni}_2\text{O}_7$ under pressure, *Phys. Rev. B* **108**, L201108 (2023).
- [51] C. Lu, Z. Pan, F. Yang, and C. Wu, Interlayer-Coupling-Driven High-Temperature Superconductivity in $\text{La}_3\text{Ni}_2\text{O}_7$ under Pressure, *Phys. Rev. Lett.* **132**, 146002 (2024).
- [52] Z.-Y. Shao, C. Lu, M. Liu, Y.-B. Liu, Z. Pan, C. Wu, and F. Yang, Pairing without γ -Pocket in the $\text{La}_3\text{Ni}_2\text{O}_7$ Thin Film, [arXiv:2507.20287](https://arxiv.org/abs/2507.20287).
- [53] T. A. Maier and D. J. Scalapino, Pairfield fluctuations of a 2D Hubbard model, *npj Quantum Materials* **4**, 1 (2019).
- [54] D. J. Scalapino, Pair Tunneling as a Probe of Fluctuations in Superconductors, *Phys. Rev. Lett.* **24**, 1052 (1970).
- [55] M. Jarrell, T. Maier, C. Huscroft, and S. Moukouri, Quantum Monte Carlo algorithm for nonlocal corrections to the dynamical mean-field approximation, *Phys. Rev. B* **64**, 195130 (2001).
- [56] W. Wu and A.-M.-S. Tremblay, d -wave superconductivity in the frustrated two-dimensional periodic Anderson model, *Phys. Rev. X* **5**, 011019 (2015).
- [57] Y.-Y. Zheng and W. Wú, s_{\pm} -wave superconductivity in the bilayer two-orbital Hubbard model, *Phys. Rev. B* **111**, 035108 (2025).
- [58] T. A. Maier, P. Doak, L.-F. Lin, Y. Zhang, A. Moreo, and E. Dagotto, Interlayer pairing in bilayer nickelates, *npj Quantum Materials* **11**, 19 (2026).
- [59] M. Shi-cong, Y. yuan. Zheng, and W. Wú, Intertwined Electron Pairing in the Bilayer Two-orbital Kanamori-Hubbard Model: a Unified Picture of Two Superconductivities in $\text{La}_3\text{Ni}_2\text{O}_7$, [arXiv:2508.04554](https://arxiv.org/abs/2508.04554).
- [60] N. P. Armitage, P. Fournier, and R. L. Greene, Progress and perspectives on electron-doped cuprates, *Rev. Mod. Phys.* **82**, 2421 (2010).
- [61] M. Kitatani, L. Si, O. Janson, R. Arita, Z. Zhong, and K. Held, Nickelate superconductors—a renaissance of the one-band hubbard model, *npj Quantum Materials* **5**, 59 (2020).
- [62] M. Kitatani, L. Si, P. Worm, J. M. Tomczak, R. Arita, and K. Held, Optimizing superconductivity: From cuprates via nickelates to palladates, *Phys. Rev. Lett.* **130**, 166002 (2023).
- [63] L. Si, E. Jacob, W. Wu, A. Hausoel, J. Krsnik, P. Worm, S. Di Cataldo, O. Janson, and K. Held, Closing in on possible scenarios for infinite-layer nickelates: Comparison of dynamical mean-field theory with angular-resolved photoemission spectroscopy, *Phys. Rev. Res.* **6**, 043104 (2024).
- [64] Y. Gao, W. Wu, Z. Liu, K. Held, and L. Si, Topotactical hydrogen induced single-band d -wave superconductivity in la_2nio_4 , *Phys. Rev. Lett.* **135**, 026002 (2025).

Supplementary material: Enhanced s^\pm -wave superconductivity in electron-doped $\text{La}_3\text{Ni}_2\text{O}_7$

Xun Liu ¹, Chao Deng ², Wenfeng Wu ², Liang Si ^{2,3,4,5} and Mi Jiang ^{1,6}

¹*Institute for Quantum Science, School of Physical Science and Technology,
Soochow University, Suzhou 215006, China*

²*School of Physics, Northwest University, Xi'an 710127, China*

³*Shaanxi Key Laboratory for Theoretical Physics Frontiers, Xi'an 710127, China*

⁴*Fundamental Discipline Research Center for Quantum Science and technology of Shaanxi Province, Xi'an 710127, China*

⁵*Institute of Solid State Physics, TU Wien, 1040 Vienna, Austria*

⁶*State Key Laboratory of Surface Physics and Department of Physics,
Fudan University, Shanghai 200433, P. R. China*

S.I. METHOD

1. Parameters from DFT calculations

The tight-binding parameters shown in Table. S1 used in this work are derived from first-principles calculations based on density functional theory (DFT) [1–4]. DFT-level structural relaxations and electronic structure calculations were performed using the PAW [5] method implemented in VASP and the FP-(L)APW method implemented in WIEN2k [6, 7], with the exchange-correlation functional treated within the GGA-PBE parameterization [8]. A dense $13 \times 13 \times 3$ k-point mesh was employed for Brillouin-zone integration of the unit cell. To construct the tight-binding model, the hopping parameters were extracted using maximally localized Wannier functions generated with the Wien2Wannier package [7].

2. Dynamical cluster approximation (DCA)

The bilayer two-orbital model is solved numerically using the dynamical cluster approximation (DCA) in combination with the continuous-time auxiliary-field (CT-AUX) quantum Monte Carlo (QMC) cluster solver [9–12]. As a celebrated many-body numerical approach, DCA accesses the thermodynamic limit observables by self-consistently embedding a finite cluster in a mean-field bath [9, 10]. Self-consistency is achieved by iterating between the cluster Green's function and a coarse-grained lattice Green's function, where the coarse-graining is performed over a patch of the Brillouin zone surrounding each cluster momentum \mathbf{K} .

Within this framework, short-range correlations inside the cluster are treated exactly using a cluster solver e.g. CT-AUX; while longer-range physics is captured approximately via the mean-field bath. Consequently, enlarging the cluster size systematically approaches the exact thermodynamic limit. The finite cluster effectively discretizes the Brillouin zone into a set of \mathbf{K} points, so that the self-energy $\Sigma(\mathbf{K}, i\omega_n)$ is taken as constant within each patch and piecewise constant across the full zone.

Quantum embedding methods like DCA typically

suffer from a less severe sign problem than finite-size QMC simulations due to the presence of the mean field. However, owing to model complexity, our calculations employ a $N_c = 8$ ($= 4 \times 2$)-site DCA cluster that includes the $(\pi, 0)$ and $(0, \pi)$ points, and also a $N_c = 2$ ($= 1 \times 2$)-site cluster for accessing the lower temperature.

TABLE S1. DFT-derived tight-binding parameters for the bilayer two-orbital model are provided for the following cases: 0 GPa, 15 GPa, and the heterostructure $\text{La}_3\text{Ni}_2\text{O}_7:\text{La}_3\text{Al}_2\text{O}_7$ at 0 GPa labeled LaNi(Al)O . And the non-interacting band structures are shown in Fig. S1. All values are expressed in units of eV.

	0 GPa	15 GPa	LaNi(Al)O
ϵ^x	0.67145	0.74378	0.36758
ϵ^z	0.36885	0.39038	-0.22759
t_1^{xx}	-0.4400	-0.4804	-0.4279
t_1^{zz}	-0.1049	-0.1166	-0.0604
t_2^{xx}	0.0723	0.0755	0.0737
t_2^{zz}	-0.0162	-0.0169	-0.0211
t_3^{xx}	-0.0526	-0.0536	-0.0452
t_3^{zz}	-0.0145	-0.0145	-0.0061
t_\perp^{xx}	0.00920	0.00815	0.00704
t_\perp^{zz}	-0.5858	-0.6296	-0.5759
t^{xz}	0.2154	0.2367	0.1813
t_\perp^{xz}	-0.025	-0.0257	-0.0270

3. Bethe-Salpeter equation (BSE)

The superconducting properties can be studied by solving the Bethe-Salpeter equation (BSE) in its

eigenvalue form in the particle-particle channel [13, 14]

$$-\frac{T}{N_c} \sum_{K'} \Gamma^{pp}(K, K') \bar{\chi}_0^{pp}(K') \phi_\alpha(K') = \lambda_\alpha(T) \phi_\alpha(K) \quad (1)$$

where $\Gamma^{pp}(K, K')$ denotes the irreducible particle-particle vertex of the effective cluster problem, with $K = (\mathbf{K}, i\omega_n)$ combining the cluster momenta \mathbf{K} and Matsubara frequencies $\omega_n = (2n + 1)\pi T$, and $\phi_\alpha(K)$ represents the eigenvector obtained by solving the BSE for the pairing symmetry of type α .

The coarse-grained bare particle-particle susceptibility

$$\bar{\chi}_0^{pp}(K) = \frac{N_c}{N} \sum_{k'} G(K + k') G(-K - k') \quad (2)$$

is obtained via the dressed single-particle Green's function,

$$G(k) \equiv G(\mathbf{k}, i\omega_n) = [i\omega_n + \mu - \varepsilon_{\mathbf{k}} - \Sigma(\mathbf{K}, i\omega_n)]^{-1} \quad (3)$$

where \mathbf{k} belongs to the DCA patch surrounding the cluster momentum \mathbf{K} . with the chemical potential μ and

$$\varepsilon_{\mathbf{k}} = \begin{bmatrix} H_{11} & H_{12} \\ H_{21} & H_{22} \end{bmatrix}$$

where

$$H_{11} = H_{22} = \begin{bmatrix} E^{xx} & E^{xz} \\ E^{xz} & E^{zz} \end{bmatrix}; H_{12} = H_{21} = \begin{bmatrix} t_{\perp}^{xx} & E_{\perp}^{xz} \\ E_{\perp}^{xz} & t_{\perp}^{zz} \end{bmatrix}$$

with

$$E^{xx/zx} = \epsilon^{x/z} + 2t_1^{xx/zx} (\cos k_x + \cos k_y) \\ + 4t_2^{xx/zx} \cos k_x \cos k_y + 2t_3^{xx/zx} (\cos 2k_x + \cos 2k_y)$$

$$E^{xz} = 2t^{xz} (\cos k_x - \cos k_y); E_{\perp}^{xz} = 2t_{\perp}^{xz} (\cos k_x - \cos k_y)$$

and $\Sigma(\mathbf{K}, i\omega_n)$ the cluster self-energy. In practice, we calculate 32 or more discrete points for both the positive and negative fermionic Matsubara frequency $\omega_n = (2n + 1)\pi T$ mesh for measuring the two-particle Green's functions and irreducible vertices. Therefore, the BSE Eq. (1) reduces to an eigenvalue problem of a matrix of size $(128N_c) \times (128N_c)$.

The pairing operator is defined as

$$\Delta_{\alpha}^{\dagger} = \frac{1}{\sqrt{N}} \sum_{\mathbf{k}} g_{\alpha}(\mathbf{k}) c_{\mathbf{k}}^{\dagger} c_{-\mathbf{k}}^{\dagger} \quad (4)$$

Here, α denotes the pairing symmetry and the s^{\pm} -wave is represented by the form factors $g_{s^{\pm}}(\mathbf{k}) = \cos k_z$.

We analyze the temperature evolution of the BSE eigenvalue $\lambda_{\alpha}(T)$ ($\alpha = s^{\pm}$). The observation of BCS-like logarithmic temperature dependence would indicate behavior analogous to that observed in the d -wave superconducting phase of the conventional single-band Hubbard model in the overdoped regime [15, 16]. Conversely, the emergence of linear or exponential temperature dependence would suggest non-BCS pairing fluctuations, similar to those characteristic of the pseudogap regime in the single-band model [15].

4. s^{\pm} -wave pair-field susceptibility

Following the usual DCA formalism [9–12], the pair-field susceptibility is defined as

$$P(T) = \frac{T^2}{N_c^2} \sum_{KK'l_m'l'_m'} g(\mathbf{K}) \bar{G}_{l_m l_m' l'_m' l'_m'}^{pp}(K, K') g(\mathbf{K}') \quad (5)$$

where $g(\mathbf{K}) = \cos k_z$ ($k_z = 0$ and π for bonding and antibonding combinations) is the form factor for s^{\pm} -wave pairing. $\bar{G}_{l_m l_m' l'_m' l'_m'}^{pp}(K, K')$ is the coarse-grained four-point two-particle Green's function for the orbital components ($l_m l_m' l'_m' l'_m'$, l_m denotes orbital $l = (d_{x^2-y^2}(x), d_{z^2}(z))$ in $m (= 1, 2)$ -th layer), so that we can decompose the pair-field susceptibility into two orbital-resolved components corresponding to the orbital components ($l_m l_m' l'_m' l'_m'$) for $l = l' = d_{x^2-y^2}(x)$ or $d_{z^2}(z)$ [17, 18]: P^x for $d_{x^2-y^2}$ orbital and P^z for d_{z^2} orbital, in order to examine their respective roles in s^{\pm} -wave pairing. The coarse-grained four-point two-particle Green's function can be evaluated by the BSE

$$\bar{G}_{l_m l_m' l'_m' l'_m'}^{pp}(K, K') = \bar{G}_{l_m l_m' l'_m' l'_m'}^{pp,0}(K, K') \delta_{K, K'} + \bar{G}_{l_m l_m' l'_m' l'_m'}^{pp,\Gamma}(K, K') \quad (6)$$

Thus, we define the non-interacting and interacting parts as [19]

$$P_0^{x/z}(T) = \frac{T^2}{N_c^2} \sum_{K, K'} \delta_{K, K'} \sum_{l_m l'_m'} g(\mathbf{K}) \bar{G}_{l_m l_m' l'_m' l'_m'}^{pp,0}(K, K') g(\mathbf{K}') \quad (7) \\ P_{\Gamma}^{x/z}(T) = \frac{T^2}{N_c^2} \sum_{K, K'} \sum_{l_m l'_m'} g(\mathbf{K}) \bar{G}_{l_m l_m' l'_m' l'_m'}^{pp,\Gamma}(K, K') g(\mathbf{K}') \quad (8)$$

In fact, the non-interacting part $P_0^{x/z}(T)$ is the coarse-grained bare particle-particle susceptibility as defined in Eq.(2). The more important interacting part $P_{\Gamma}^{x/z}(T)$ can be obtained as

$$\bar{G}_{l_m l_m' l'_m' l'_m'}^{pp,\Gamma}(K, K') = \frac{T}{N_c} \sum_{K, K'} \sum_{l_m^1 l_m^2 l_m^3 l_m^4} \bar{G}_{l_m^1 l_m^2 l_m^3 l_m^4}^{pp,0}(K, K') \\ \times \Gamma_{l_m^1 l_m^2 l_m^3 l_m^4}(K, K') \bar{G}_{l_m^3 l_m^4 l'_m' l'_m'}^{pp,0}(K, K') \quad (9)$$

where $\Gamma_{l_m^1 l_m^2 l_m^3 l_m^4}(K, K')$ is the reducible four-point vertex [20]. To access sufficiently low temperature, we evaluate the pair-field susceptibility using the smallest $N_c = 1 \times 2$ cluster for moderate QMC sign problem.

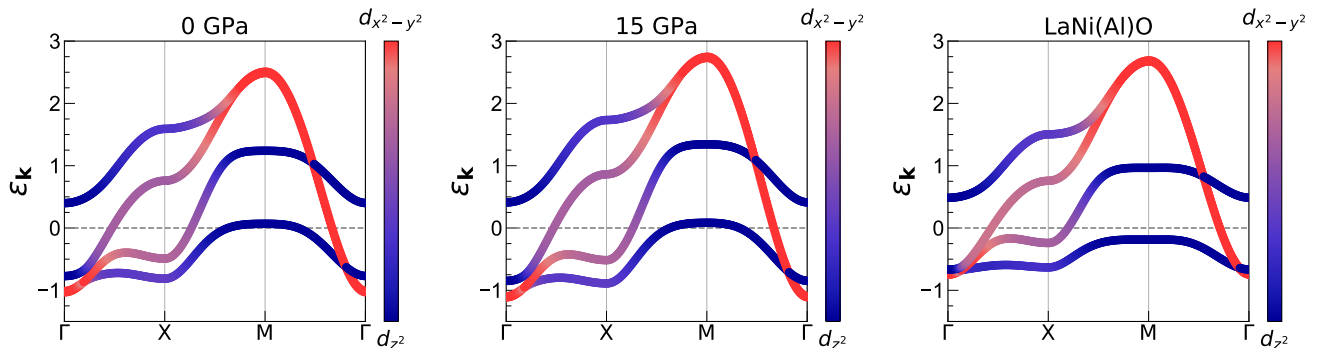


FIG. S1. Non-interacting band structures at $\delta = 0$ for three cases: 0 GPa (left), 15 GPa (middle), and LaNi(Al)O (right).

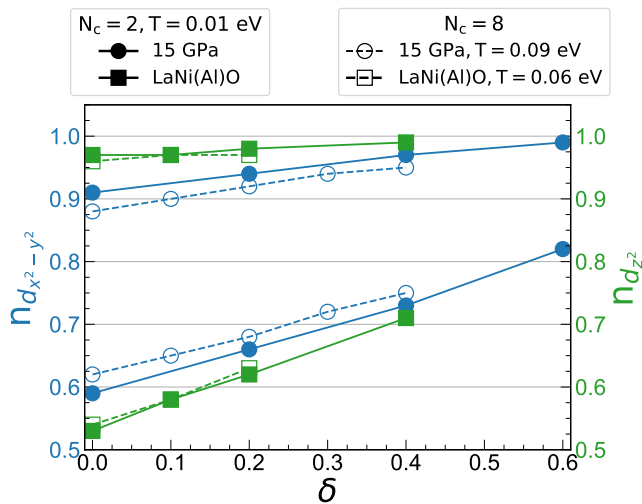


FIG. S2. Electron doping evolution of orbital occupancy for the 15 GPa (circles) and LaNi(Al)O (squares) cases at the respective lowest achievable temperatures.

S.II. DENSITY DISTRIBUTION

Fig. S1 shows the non-interacting band structures obtained from DFT parameters in Table S1 for the 0 GPa and 15 GPa cases, where the bonding (γ band) of the d_{z^2} orbital at $M = (\pi, \pi)$ is higher in the 15 GPa case than in the 0 GPa case and both cross the Fermi level. In contrast, the γ band of LaNi(Al)O lies below the Fermi level, implying larger electron occupation of the d_{z^2} orbital at the same electron density compared to the two former cases.

Fig. S2 displays the orbital occupancy for the $N_c = 1 \times 2$ and $N_c = 4 \times 2$ clusters at their lowest accessible temperatures for the 15 GPa and LaNi(Al)O cases, which confirms the expected density distribution discussed above. For the 15 GPa case, although the density distributions differ between the two clusters, the orbital occupancies for both orbitals increase with the electron doping level δ , with more doped electrons residing on the $d_{x^2-y^2}$ orbital. In contrast, for LaNi(Al)O, the density of

the d_{z^2} orbital (≈ 0.97) remains almost unchanged with δ .

S.III. EIGENVECTOR WEIGHT FOR $N_c = 1 \times 2$

In the main text, the characteristic eigenvector weight shown in Fig. 5(c) suggests an inter-orbital cooperative mechanism underlying the superconducting instability. Specifically, the interlayer pairing hosted by the $d_{x^2-y^2}$ orbital emerges below a crossover temperature (≈ 0.08 eV) for $\delta = 0.2$ in the 15 GPa case. As shown in Fig. S3 for the 15 GPa case, this temperature scale increases with electron doping level. However, for the LaNi(Al)O case shown in Fig. S4, the crossover temperature remains almost unchanged from $\delta = 0.0$ to 0.4. These distinct tendencies can be partly understood via the doping dependent d_{z^2} orbital occupancy shown in Fig. S2, where $n_{d_{z^2}}$ gradually increases towards to half-filling with δ for 15 GPa case while the LaNi(Al)O case has almost unchanged near half-filling occupancy. In this manner, near-half-filling occupancy promotes the interlayer pairing of the d_{z^2} orbital so that possesses the higher onset temperature for inducing interlayer pairing on the $d_{x^2-y^2}$ orbital. Moreover, a large density close to half-filling on the d_{z^2} orbital is beneficial for the interlayer pairing owing to the strong local moment for the interlayer singlet formation.

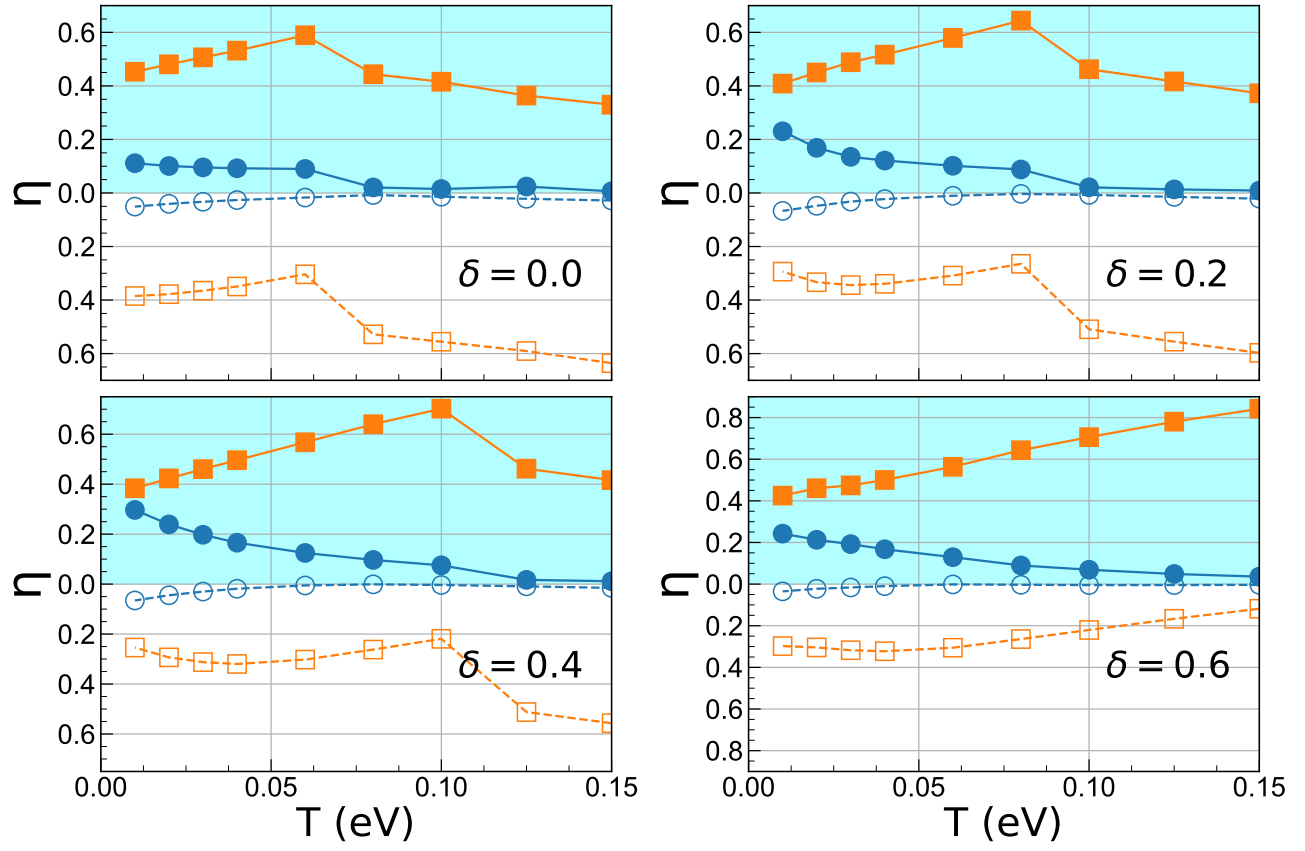


FIG. S3. Eigenvector weights as a function of doping $\delta = 0.0, 0.2, 0.4$ and 0.6 for the 15 GPa case.

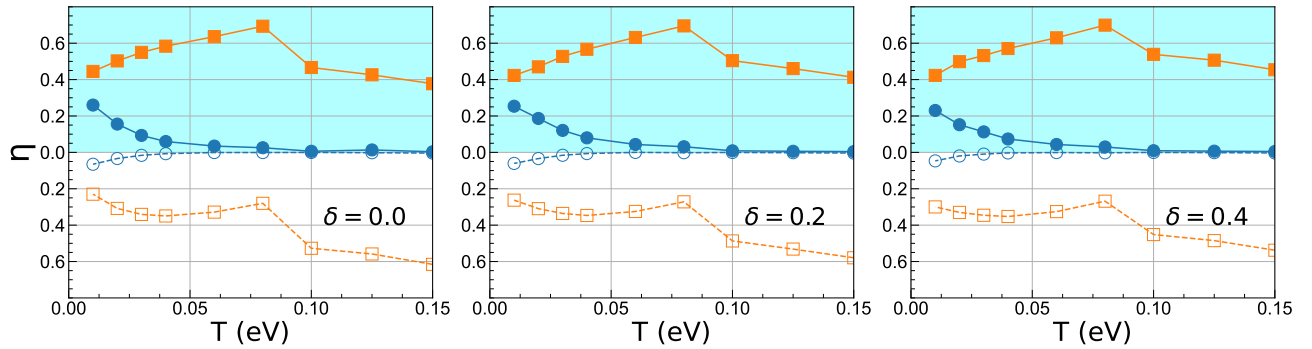


FIG. S4. Akin to Fig. S3, but for the LaNi(Al)O case. Eigenvector weights as a function of doping $\delta = 0.0, 0.2,$ and 0.4 .

-
- [1] P. Hohenberg and W. Kohn, Inhomogeneous Electron Gas, *Phys. Rev.* **136**, B864 (1964).
- [2] W. Kohn and L. J. Sham, Self-Consistent Equations Including Exchange and Correlation Effects, *Phys. Rev.* **140**, A1133 (1965).
- [3] G. Kresse and J. Furthmüller, Efficiency of ab-initio total energy calculations for metals and semiconductors using a plane-wave basis set, *Computational Materials Science* **6**, 15 (1996).
- [4] G. Kresse and J. Furthmüller, Efficient iterative schemes for ab initio total-energy calculations using a plane-wave basis set, *Phys. Rev. B* **54**, 11169 (1996).
- [5] P. E. Blöchl, Projector augmented-wave method, *Phys. Rev. B* **50**, 17953 (1994).
- [6] P. Blaha, K. Schwarz, G. Madsen, D. Kvasnicka, and J. Luitz, *Wien2k: An augmented plane wave plus local orbitals program for calculating crystal properties* (2001).
- [7] K. Schwarz, P. Blaha, and G. Madsen, Electronic structure calculations of solids using the WIEN2k package for material sciences, *Computer Physics Communications* **147**, 71 (2002), proceedings of the Europhysics Conference on Computational Physics Computational Modeling and Simulation of Complex Systems.
- [8] J. P. Perdew, K. Burke, and M. Ernzerhof, Generalized Gradient Approximation Made Simple, *Phys. Rev. Lett.* **77**, 3865 (1996).
- [9] M. H. Hettler, A. N. Tahvildar-Zadeh, M. Jarrell, T. Pruschke, and H. R. Krishnamurthy, Nonlocal dynamical correlations of strongly interacting electron systems, *Phys. Rev. B* **58**, R7475 (1998).
- [10] T. Maier, M. Jarrell, T. Pruschke, and M. H. Hettler, Quantum cluster theories, *Rev. Mod. Phys.* **77**, 1027 (2005).
- [11] U. R. Hähner, G. Alvarez, T. A. Maier, R. Solcà, P. Staar, M. S. Summers, and T. C. Schulthess, DCA++: A software framework to solve correlated electron problems with modern quantum cluster methods, *Computer Physics Communications* **246**, 106709 (2020).
- [12] E. Gull, P. Werner, O. Parcollet, and M. Troyer, Continuous-time auxiliary-field monte carlo for quantum impurity models, *Europhysics Letters* **82**, 57003 (2008).
- [13] T. A. Maier, M. S. Jarrell, and D. J. Scalapino, Structure of the pairing interaction in the two-dimensional Hubbard model, *Phys. Rev. Lett.* **96**, 047005 (2006).
- [14] D. J. Scalapino, *Handbook of High-Temperature Superconductivity: Theory and Experiment* (Springer, New York, NY, 2007) pp. 495–526.
- [15] T. A. Maier and D. J. Scalapino, Pairfield fluctuations of a 2D Hubbard model, *npj Quantum Materials* **4**, 1 (2019).
- [16] D. J. Scalapino, Pair Tunneling as a Probe of Fluctuations in Superconductors, *Phys. Rev. Lett.* **24**, 1052 (1970).
- [17] W. Wu and A.-M.-S. Tremblay, *d*-wave superconductivity in the frustrated two-dimensional periodic Anderson model, *Phys. Rev. X* **5**, 011019 (2015).
- [18] Y.-Y. Zheng and W. Wú, *s_±*-wave superconductivity in the bilayer two-orbital Hubbard model, *Phys. Rev. B* **111**, 035108 (2025).
- [19] T. A. Maier, P. Doak, L.-F. Lin, Y. Zhang, A. Moreo, and E. Dagotto, Interlayer pairing in bilayer nickelates, *npj Quantum Materials* **11**, 19 (2026).
- [20] M. Jarrell, T. Maier, C. Huscroft, and S. Moukouri, Quantum Monte Carlo algorithm for nonlocal corrections to the dynamical mean-field approximation, *Phys. Rev. B* **64**, 195130 (2001).